# Three interaction energy scales in the single-layer high-$T_c$ cuprate HgBa$_2$CuO$_{4+\delta}$

S. A. Sreedhar,[1] A. Rossi ®,[1,2] J. Nayak ®,[1,*] Z. W. Anderson,[3] Y. Tang,[3] B. Gregory,[4] M. Hashimoto,[5] D.-H. Lu ®,[5]
E. Rotenberg ®,[2] R. J. Birgeneau ®,[6] M. Greven,[3] M. Yi,[7,6] and I. M. Vishik ®[1,†]

[1]*Department of Physics and Astronomy, University of California, Davis, California 95616, USA*
[2]*Advanced Light Source, Lawrence Berkeley National Lab, Berkeley, California 94720, USA*
[3]*University of Minnesota, School of Physics and Astronomy, Minneapolis, Minnesota 55455, USA*
[4]*Cornell University, Department of Physics, Ithaca, New York 14850, USA*
[5]*Stanford Synchrotron Radiation Lightsource, SLAC National Accelerator Laboratory, Menlo Park, California 94025, USA*
[6]*Department of Physics, University of California, Berkeley, California 94720, USA*
[7]*Department of Physics and Astronomy, Rice University, Houston, Texas 77005, USA*

The lamellar cuprate superconductors exhibit the highest ambient-pressure superconducting transition temperatures ($T_c$), and after more than three decades of extraordinary research activity, continue to pose formidable scientific challenges. A major experimental obstacle has been to distinguish universal phenomena from materials- or technique-dependent ones. Angle-resolved photoemission spectroscopy (ARPES) measures momentum-dependent single-particle electronic excitations and has been invaluable in the endeavor to determine the anisotropic momentum-space properties of the cuprates. HgBa$_2$CuO$_{4+\delta}$ (Hg1201) is a single-CuO$_2$-layer cuprate with a particularly high optimal $T_c$ and a simple crystal structure, yet there exists little information from ARPES about the electronic properties of this model system. Here we present an ARPES study of doping-, temperature-, and momentum-dependent systematics of near-nodal dispersion anomalies in Hg1201. The data reveal a hierarchy of three distinct energy scales: a subgap low-energy kink, an intermediate-energy kink near 55 meV, and a peak-dip-hump structure. The first two features are attributed to the coupling of electrons to Ba-derived optical phonons and in-plane bond-stretching phonons, respectively. The nodal peak-dip-hump structure appears to have a common doping dependence in several single-layer cuprates and is interpreted as a manifestation of pseudogap physics at the node. These results establish several universal phenomena, both in terms of connecting multiple experimental techniques for a single material and in terms of connecting comparable spectral features in multiple structurally similar cuprates.

## I. INTRODUCTION

Cuprate high-temperature superconductors have a rich phase diagram with multiple competing and coexisting phenomena and interactions, which are characterized by strong anisotropy both in real space and momentum space [1–5], the latter of which is the focus of this work. Many of these emergent phases, notably superconductivity and the normal state pseudogap, remain without an accepted microscopic explanation, and one promising approach is to identify associated collective excitations to which electrons strongly couple. Doing so often requires multiple experimental probes, but different compounds are often favored by different techniques, muddling this correspondence.

The cuprates share a common structural unit of the CuO$_2$ plane, but the hundreds of known cuprate compounds differ from one another in the number of adjacent CuO$_2$ planes (single layer vs multiple layer) and in the chemistry of the charge reservoir layers separating CuO$_2$ plane(s) from one another. While a common framework is the goal, disparities among compounds can also guide an understanding of the mechanism that gives rise to pairing and/or enhances $T_c$.

Nowhere is this materials dependence more striking than among single-layer cuprates. These materials are structurally similar, but some have maximum $T_c$ values ($T_{c,\max}$) near 35–40 K, whereas others have $T_{c,\max}$ near 100 K [6–9]. There has been recent systematic characterization of higher-energy band structure, with implications for interpreting this variation in $T_c$ [10,11]. Low-energy momentum-dependent many-body interactions are relatively well characterized in several of the lower-$T_c$ compounds [12–14]. This helps guide interpretation of bulk phenomena in terms of momentum-dependent microscopic electronic properties, but few comparable systematic ARPES studies exist as yet for any of the higher-$T_c$ members, aside from a small number of studies on Tl$_2$Ba$_2$CuO$_{6+\delta}$ (Tl2201) in the overdoped regime [15,16].

HgBa$_2$CuO$_{4+\delta}$ (Hg1201) has $T_{c,\max} = 98$ K and is considered to be a model cuprate because of its single-layer simple-tetragonal crystal structure and relatively minor (point) disorder effects [6,17]. It is also a member of the family of Hg cuprates which achieves the maximum $T_c$ among all

*Present address: Department of Physics, Indian Institute of Technology Kanpur, Kanpur - 208016, India.
†ivishik@ucdavis.edu

cuprates in the triple-layer version [18]. There exist extensive experimental results for Hg1201, including charge transport [19,20], torque magnetometry [21], optical spectroscopy [22], microwave [23], as well as neutron [24–26], x-ray [27–29], and Raman [30] scattering. However, ARPES measurements have been limited owing to the lack of a neutral cleavage plane and the high sensitivity to photoemission matrix elements [31].

Here we present a systematic (doping-, temperature-, momentum-dependence) study of near-nodal dispersions and lineshapes that highlights three different energy scales in the ARPES spectra of Hg1201 and establishes key points of universality and deviations thereof among single-layer cuprates. First, we observe a low-energy kink (at $\omega \approx 11$ meV), which has so far been reported only for Bi-based cuprates and associated with the interaction of electrons with acoustic or optical phonons [32–36]. Second, the intermediate-energy kink ($\omega \approx 55$ meV) shows a temperature, doping, and momentum-dependent phenomenology consistent with coupling to in-plane bond-stretching phonons. While this appears to be common to all single-layer cuprates, the stronger coupling in Hg1201 suggests a possible connection to $T_c$ enhancement. Finally, a peak-dip-hump (PDH) lineshape is observed at the *node*, the momentum point where the superconducting gap is identically zero. We find that the nodal PDH also has a doping dependence similar to that of the pseudogap, the anomalous state existing above $T_c$ in hole doped cuprates. The nodal PDH appears to be ubiquitous in single-layer cuprates and may be connected to significant electronic changes at the hole-doping level $p \approx 0.2$, favoring explanations of pseudogap phenomena which do not vanish at the node. Hg1201 has yielded important insights from multiple experimental techniques, and the comprehensive nature of the present ARPES work contributes to establishing a cohesive multitechnique narrative about this prototype material.

## II. EXPERIMENTS

Hg1201 single crystals were grown by a two-step flux method [37] and were subsequently annealed to achieve the desired $T_c$ [17]. For ARPES experiments, care was taken to ensure mechanical adhesion and electrical conductance between the samples and the sample holder, because Hg1201 is mechanically robust and reacts with commonly used silver epoxies. Samples were glued onto the copper sample post using Torr seal. Silver paint (DuPont 4922N-100) was used to ground the samples and was cured at room temperature. ARPES experiments were performed at Stanford Synchrotron Radiation Lightsource (SSRL) beamline 5-4 using 19.4 eV photon energy, which was previously shown to optimize valence band spectral quality near the node [31]. The beam-spot size was approximately 100 microns. Samples were cleaved *in situ* at the lowest measurement temperature (30 K). Roughness of the cleaved surface can contribute to extrinsic broadening of ARPES lineshapes, and the quality of the cleave was assessed from the presence of a quasiparticle peak and the Lorentzian width of the momentum distribution curve (MDC) at $E_F$, which was as small as 0.09 Å$^{-1}$. Additional x-ray photoelectron spectroscopy (XPS) measurements were performed at beamline 7.0.2 of the Advanced Light Source
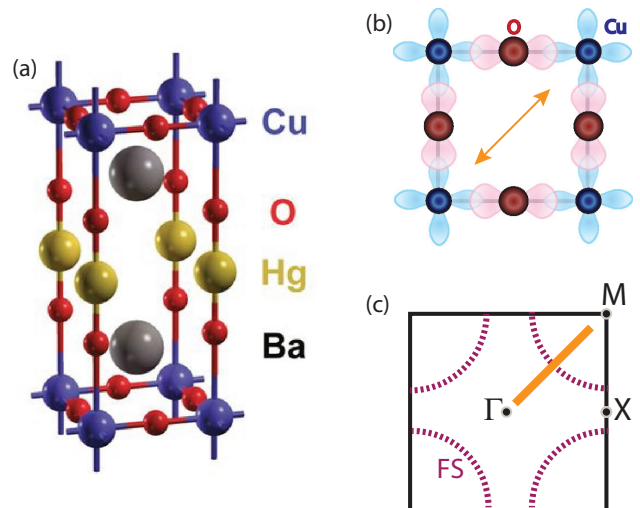


FIG. 1. Crystal structure and Brillouin zone of Hg1201. (a) Schematic crystal structure of Hg1201 for simplicity drawn without oxygen interstitials in the Hg layers. Image from Ref. [19]. (b) portion of $CuO_2$ plane, with bond-diagonal (nodal) direction indicated by orange arrow. (c) Two-dimensional projection of tetragonal Brillouin zone with high-symmetry points labeled. Schematic of Fermi surface (FS) is shown by purple dashed line, with nodal cut indicated by thick orange line.

(ALS) to ascertain surface termination, and these data are shown in the Appendix.

## III. RESULTS

The unit cell of Hg1201 [Fig. 1(a)] has a single $CuO_2$ plane. Our XPS measurements suggest that cleavage happens at the O-Hg-O barbells (Appendix), which are located relatively far from $CuO_2$ planes and yield an overall neutral cleaved surface, because the bond is equally likely to be broken above ($Hg^{2+}$ termination) and below ($O^{2-}$ termination) the Hg atoms. The nodal cuts considered for the majority of this paper correspond to 45° from the Cu-O bond directions in the $CuO_2$ plane [Fig. 1(b)] or along the diagonal of the Brillouin zone [Fig. 1(c)]. The terminology originates from the zero of the superconducting gap, but it is used even in the absence of superconductivity to refer to the aforementioned trajectory.

Figure 2 shows dispersions and lineshapes along nodal cuts for the three doping levels investigated in this study: UD70 (underdoped, $T_c = 70$ K, $p \approx 0.095$), UD80 ($p \approx 0.11$), and OP98 (optimal doping, $p \approx 0.16$), with doping levels estimated from Ref. [38]. All data in this figure were obtained at 30 K, which is well below $T_c$. An incoherent background was subtracted to obtain image plots [Figs. 2(a), 2(d) and 2(g)]. Dispersions are quantified by fitting MDCs to Lorentzians plus a constant background, and the results, with a focus on the lower-energy anomalies, are shown in Figs. 2(b), 2(e) and 2(h). The ubiquitous dispersion kink is observed around 50–70 meV, and its estimated energy is indicated by arrows. Another bend in the dispersion, the low-energy kink, is observed at $\approx 11$ meV. An assumed tight-binding bare band [39,40] is also shown in panels (b), (e), and (h), and discussed
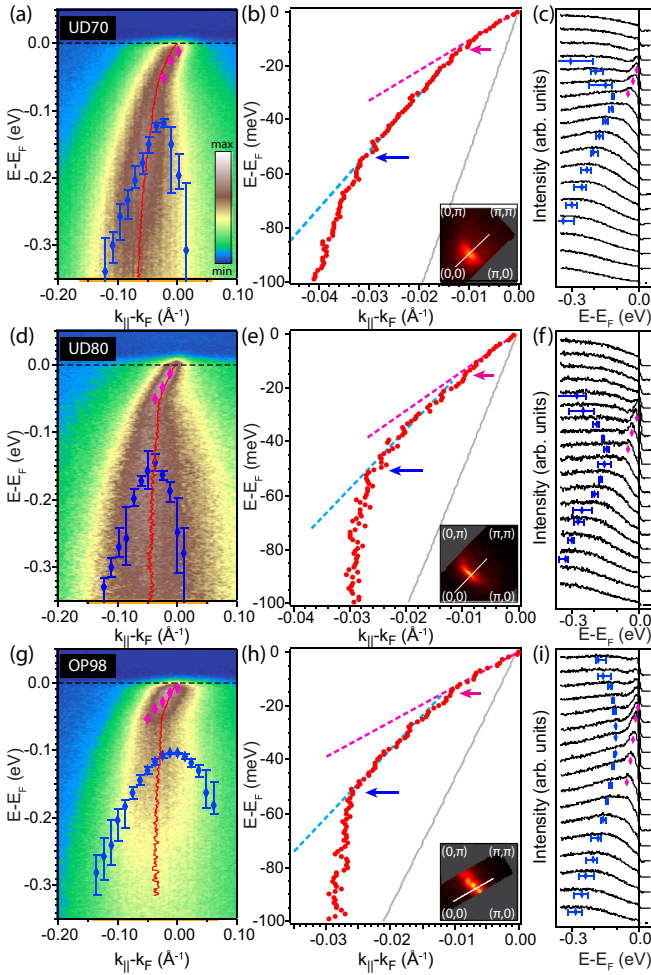
FIG. 2. Nodal dispersions and lineshapes, $T = 30$ K. (a) Nodal cut for UD70. Red line: MDC-fitted dispersion. Magenta and blue symbols: 'peak' and 'hump' positions (local maxima). Incoherent background, determined from EDC far from the dispersion, has been subtracted. (b) MDC-derived dispersion for UD70. Thin gray line: tight-binding band dispersion, used as bare band. Magenta and cyan dotted lines: linear fits between $[0, -10]$ meV and $[-25, -45]$ meV, respectively. Magenta and blue arrows point to the low-energy and intermediate-energy kinks, respectively. Inset: measured Fermi surface and cut angle (white). (c) EDCs for UD70 along momentum region marked by orange bar in (a), with peak and hump positions indicated. (d)–(f) Same data for UD80. (g)–(i) Same data for OP98. All measurements are taken at 30 K. Error bars in hump position reflect variation in eight adjacent EDCs, which were averaged to give each EDC in (c), (f), and (i).

further in the Supplemental Material (SM) [41]. All dopings use the same tight-binding parameters, yielding a bandwidth of 1.36 eV, with chemical potential adjusted to match nominal doping. Energy distribution curves (EDCs) along the momentum range marked by orange bars in panels (a), (d), and (g) are shown in Figs. 2(c), 2(f) and 2(i). Quasiparticle peaks are observed near $k_F$ at all three doping levels (magenta), which attests to the quality of the spectra. An additional 'hump' feature is observed at higher binding energy, lending a PDH lineshape to *nodal* cuts even at optimal doping. The peak and hump energies were determined from local maxima of

smoothed data. The 'hump' feature first disperses toward the Fermi energy ($E_F$) and then disperses away. The two nodal kinks and the nodal PDH structure provide evidence for strong interactions at three distinct characteristic energy scales.

Energies and coupling strengths of the intermediate energy kink can be quantified via the real part of the self energy (Re$\Sigma$) (Fig. 3). This quantity is estimated by subtracting an assumed tight-binding bare band from the MDC dispersion, a standard technique to assess the effects of many-body interactions on band position [42–45]. The momentum difference at each energy is multiplied by the slope of the bare band, which is nearly linear in the energy region of interest, to recover units of energy. The kink energy is estimated from the broad peak of Re$\Sigma$ and slightly disperses to lower energy with increasing doping at 30 K [Figs. 3(a), 3(d) and 3(g)]. Additionally, a subkink feature is observed around 11 meV, consistent with the low-energy kink previously only reported in Bi-based cuprates [5,32–35,46]. Temperature dependence of Re$\Sigma$ is shown in panels (b), (e), and (h) for UD70, UD80, and OP98, respectively. For all dopings, data are shown well below $T_c$ and well above $T_c$, and for UD70 and UD80, data are shown slightly above $T_c$ additionally. For the dopings in this study, the pseudogap temperature ($T^*$) [19,26] could not be accessed because of sample aging above 200 K. For all three dopings, Re$\Sigma$ appears to be relatively insensitive to temperature, decreasing by less than 20% at its maximum between low temperature and well above $T_c$. We note that for the OP98 data set, temperature-dependent data [Fig. 3(h)] were taken the node opposite from low temperature data [Fig. 3(g)], and the different magnitude of Re$\Sigma$ is likely due to a slight misalignment between the two measurements. Additional temperature-dependence data is in the SM [41]. Figures 3(c), 3(f) and 3(i) show the momentum dependence of Re$\Sigma$ at 30 K starting at the node (red) and moving approximately 1/3 of the way to the antinode (dark blue). The momentum dependence is more substantial than the temperature dependence, with the magnitude of Re$\Sigma$ decreasing by at least 75% over the aforementioned momentum range.

We now turn to the nodal PDH structure. Figure 4(a) shows the EDCs at the nodal $k_F$ for the three doping levels, indicating that the nodal PDH persists to at least optimal doping. The dip feature persists above $T_c$ and is shown for UD70 in panel (b). The hump energy scale disperses to higher energy moving away from the node, as shown for OP98 in Figs. 4(c) and 4(d), and extrapolates to an antinodal energy scale of $\approx 300$ meV.

## IV. DISCUSSION

We first address the low-energy kink. A similar feature was previously observed and studied in Bi-based cuprates. It was found that the velocity renormalization across this kink increases with underdoping below a certain material-dependent hole concentration ($p \approx 0.13$ in $Bi_2Sr_2CaCu_2O_{8+\delta}$ (Bi2212) [33] and $p \approx 0.2$ in $Bi_2Sr_2CuO_{6+\delta}$ (Bi2201) [34]). In Hg1201, we obtain a velocity renormalization, $v_{mid}/v_F \approx 2$, for all studied doping levels, where $v_F$ is the slope of the MDC dispersion 0–10 meV and $v_{mid}$ is the slope in the 20–45 meV range. These energy intervals are chosen to avoid low-energy and intermediate-energy kinks. This suggests that
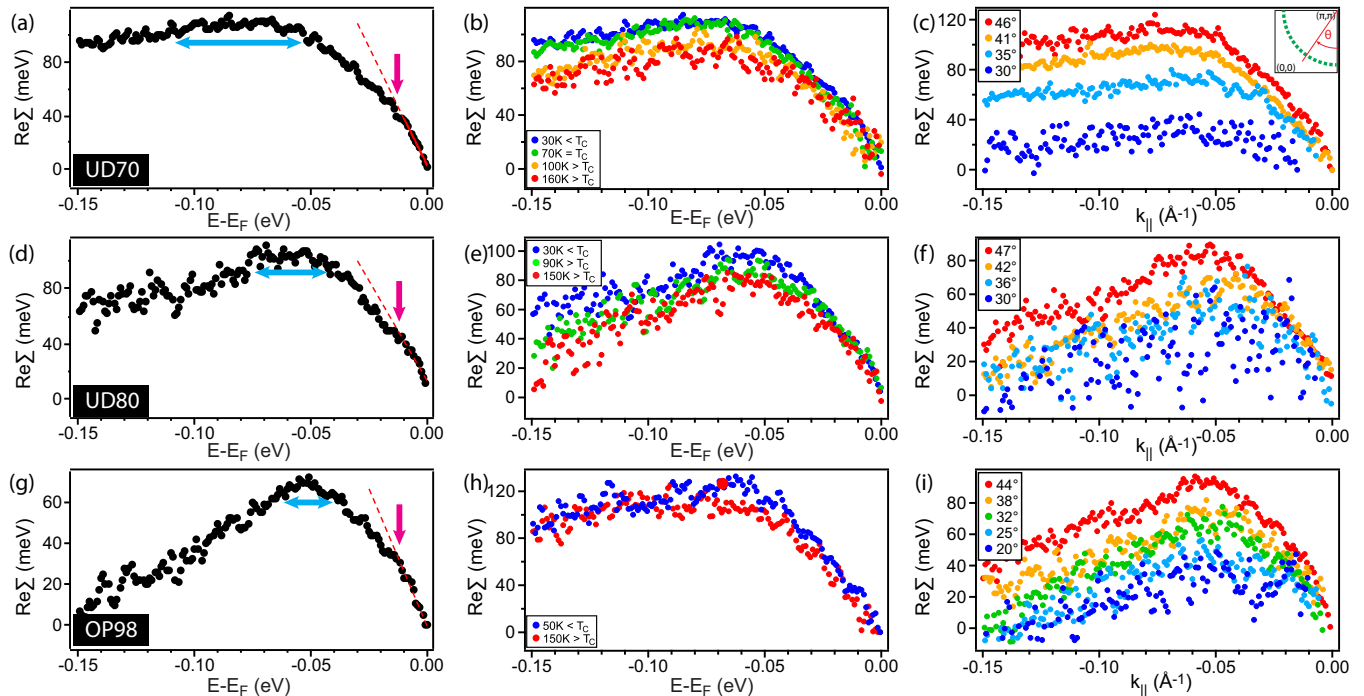
FIG. 3. Doping, temperature, and momentum dependence of the real part of the self energy, $\mathrm{Re}\Sigma$, derived by subtracting assumed tight-binding bare band. $T = 30$ K unless otherwise stated. (a) $\mathrm{Re}\Sigma$ at the node for UD70. Blue arrow indicates the energy range of the intermediate energy kink for each doping corresponding to a 15% decrease of $\mathrm{Re}\Sigma$ from the maximum value. Dashed red line is a linear fit to the low energy (0–10 meV) portion of $\mathrm{Re}\Sigma$. Deviation from this linear fit suggests a low energy kink indicated by the magenta arrow. (b) Temperature dependence of $\mathrm{Re}\Sigma$ at the node, UD70. (c) Momentum dependence of $\mathrm{Re}\Sigma$ for UD70 showing the weakening of the kink away from node, with angle as indicated in the inset. (d)–(f) Same measurements for UD80. (g)–(i) Same measurements for OP98.

doping dependence, if present in Hg1201, occurs at lower hole concentrations than accessed by this study; alternately the mechanism of the low-energy kink in this system may be different from Bi-based cuprates. Additionally, the velocity renormalization at optimal doping in Hg1201 is approximately 20% more than what is observed in Bi2201 [34], suggesting that the excitation responsible for the low-energy kink may contribute to the enhanced $T_c$.

The low-energy kink in Bi-based cuprates has been attributed to coupling to either acoustic [36] or optical phonons [32], with proposed electron-phonon coupling peaked at small **q** for both cases. Our assignment for Hg1201 is guided by phonon dispersions measured near optimal doping [47,48] and by the kink energy that we observe. A kink at 11 meV is consistent with a zone-center $c$-axis optical branch, and with in-plane ($E_u$) modes at large momentum transfer, but not with acoustic phonons, which reach a maximum of only $\approx 7$ meV at the zone boundary [47]. The calculated phonon density of states shows contributions primarily from Ba in the energy range of interest [47]. It has been shown that only $A_{1g}$-symmetry optical phonons can have coupling peaked at **q** = 0 for nodal fermions, and the closest candidate in Hg1201 is a Ba mode with energy 20–26 meV [47,49]. This is a bit higher than low-energy kink energy, but it is possible that the phonon frequency softens near the sample surface. Electron-phonon coupling peaked at larger **q** needs to be considered as well, which points to Ba-derived optical modes with large reduced momentum. As we will discuss later, the lack of a gap shift can be achieved by scattering from near node to near node.

This mechanism is different from most explanations of the low-energy kink in Bi-based cuprates and may be related to the different doping dependence of this feature in Hg1201.

The intermediate-energy nodal kink, observed between 50–80 meV in all cuprates [5,50,51], is a ubiquitous spectral feature with various purported origins. It has been attributed to a coupling to sharp bosonic excitations of lattice [50,52], magnetic or electronic [53,54], or dual origin [55]. There also exist proposals that involve coupling to a gapped continuum of excitations [56] and proposals that do not involve electron-boson coupling [57]. Notably, in the present data, the MDC-derived dispersions for nodal cuts show a slight 'S' shape, most visible in Fig. 5(a), the characteristic of coupling to a sharp bosonic mode [56].

In Hg1201, several previously reported excitations have energy scales similar to the intermediate-energy kink: a dispersionless Ising-like excitation [58], the maximum in the magnetic susceptibility at the antiferromagnetic wave vector [25,26], and bond-stretching in-plane phonons [48]. Additionally, a recent x-ray scattering study of an underdoped $T_c = 70$ K Hg1201 sample revealed a broad spectrum of charge excitations in the vicinity of the two-dimensional wave vector $\mathbf{q}_{\mathrm{CDW}} = (0.3, 0)$, where short-range charge order is observed, but these excitations are peaked at energies smaller than the kink energy [59].

The intermediate-energy nodal kink is a somewhat broad feature, particularly in the underdoped regime, possibly with multiple (lattice, magnetic, charge) contributions, and here we narrow down the likeliest phonon contribution based on
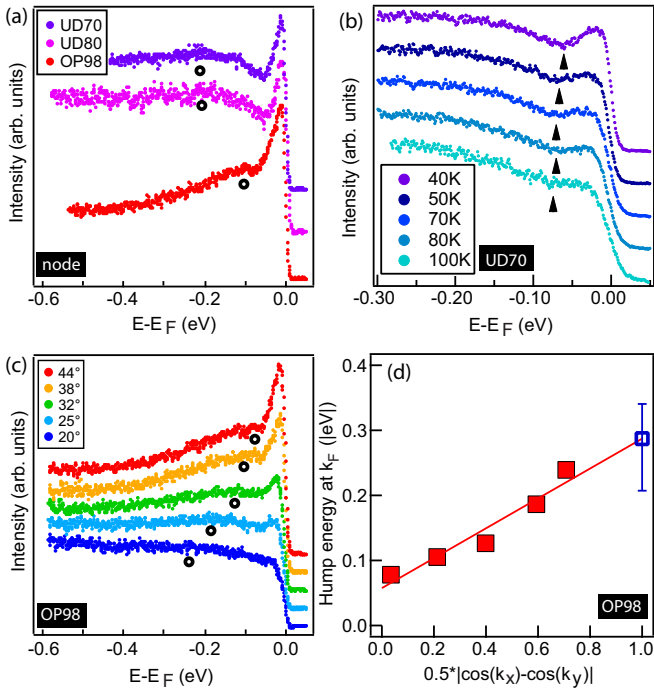
FIG. 4. Nodal peak-dip hump. $T = 30$ K unless otherwise stated. (a) Doping dependence at the node ($k_F$), normalized by maximum intensity and offset for clarity. (b) Temperature dependence at $k_F$, UD70. Normalized at $-0.25$ eV and offset for clarity. Arrow indicates the dip. (c) Momentum dependence for OP98, showing EDCs at $k_F$. Markers point to the hump energy as defined in Fig. 2. EDCs normalized at $-0.55$ eV and offset for clarity. (d) Momentum dependence of hump energy scale in (c) plotted as a function of simple $d$-wave form and extrapolated to antinode. Blue marker is the extrapolated value with lower and upper error bar indicating the range of extrapolated value using the first three and last three data points, respectively.

observed phenomenology. As noted, in Hg1201, this kink appears to have some doping dependence [see Figs. 3(a), 3(d) and 3(g)]. At optimal doping, its energy is approximately 55 meV. For UD70, although the feature is broader, its characteristic energy is closer to 70 meV. This doping dependence is the opposite of that of the maximum in the local magnetic susceptibility in Hg1201 ($\sim$55 meV and $\sim$60 meV for samples with $T_c = 71$ K and 88 K, respectively) [25,26] and other cuprates [65], which decreases with underdoping. The Ising-like excitations have not been observed in cuprates other than Hg1201, and the energy of the higher energy branch exhibits little doping dependence and strong temperature dependence [58,66]. We will therefore not discuss them further.

On the other hand, the bond-stretching phonon along [100] is generally found to shift to lower energy (soften) approaching the middle of the Brillouin zone [$\mathbf{q} = (0.5, 0, 0)$ and equivalent] in doped cuprates, which has been interpreted as evidence of strong coupling to electrons [67]. Whereas doping dependence is not well established for Hg1201 at this time, the bond-stretching phonon energy at $\mathbf{q} = (0.5, 0, 0)$ has been shown to decrease systematically with increasing doping in La$_{2-x}$Sr$_x$CuO$_4$ (LSCO), while the energy of this branch near $\mathbf{q} = (0, 0, 0)$ has minimal doping dependence [63]. In

Hg1201, both at optimal doping [48] and for an underdoped sample with $T_c = 55$ K [68], the measured energy of the bond-stretching phonon at $\mathbf{q} = (0.5, 0, 0)$ is consistent with the energy of the intermediate-energy kink in Figs. 3(a), 3(d) and 3(g). Further connections will be made when we discuss the momentum dependence.

The second consideration is the minimal or absent temperature dependence of the kink, including the lack of a shift to lower energy across $T_c$ [Figs. 3(b), 3(e) and 3(h)]. In a $d$-wave superconductor, a kink observed at energy $\omega$ will generally be associated with a phonon of energy $\Omega = \omega - \Delta_0$, where $\Delta_0$ is the maximum of the superconducting gap, if the momentum-dependent electron-phonon coupling connects the momentum of interest to the momentum where the superconducting gap is maximum [69]. The maximum of the superconducting gap of Hg1201 has previously been measured to be around 39 meV at optimal doping [31]. However, there are exceptions to this expectation of 'gap shifting,' e.g., when electron-phonon coupling is strongly peaked in the forward direction ($\mathbf{q} \approx 0$) such that fermions at a given momentum are only sensitive to the gap local to that momentum point [36], or if the coupling is strongly peaked at a particular momentum transfer that connects momenta with zero or small gap, such as two opposite nodes. The latter is consistent with the momentum dependence in the present data [Figs. 3(c), 3(f) and 3(i)], as will be discussed later. The minimal temperature dependence of the magnitude of Re$\Sigma$ in Fig. 3 suggests a lattice origin of the intermediate-energy kink, and the lack of gap shifting of the peak position of Re$\Sigma$ restricts this to phonon modes with strongly $\mathbf{q}$-dependent coupling.

There exists some materials dependence with regard to the nodal kink phenomenology. For example, Bi2212 shows a strong temperature dependence of the coupling strength, primarily across $T_c$ [43], but also extending to higher temperature [70], whereas other single-layer cuprates show weaker or absent temperature dependence similar to Hg1201 [71,72]. This is consistent with additional contributions to the nodal kink in multi-CuO$_2$-plane cuprates, such as coupling to the $B_{1g}$ (buckling) mode [73].

There is also variation among single-layer cuprates with regard to the energy position of the intermediate-energy kink, which closely tracks variation in the energy of the [100] bond-stretching mode at large momentum transfer. Figure 5(a) compares the intermediate-energy nodal kink near optimal doping for several single-layer cuprates: Hg1201, Ca$_{2-x}$Na$_x$CuO$_2$Cl$_2$ (Na-CCOC), LSCO, and Bi2201. Also shown are the values for the bond-stretching (half-breathing) phonon at $\mathbf{q} = (0.5, 0, 0)$ near optimal doping [48,62–64]). Notably, for all single-layer cuprates near optimal doping, the bond-stretching phonon energy at $\mathbf{q} = (0.5, 0, 0)$ is lower by 10–15 meV than at the zone center, more consistent with the energy of the intermediate-energy kink, which further constrains the origin of this feature to the soft part of this phonon branch.

The third aspect of the intermediate-energy kink phenomenology is the pronounced momentum dependence shown in Figs. 3(c), 3(f) and 3(i), with the kink nearly disappearing for cuts sufficiently far from the node. This suggests a strong anisotropy in either the mode or the coupling or both. As discussed in prior work [64], this momentum dependence
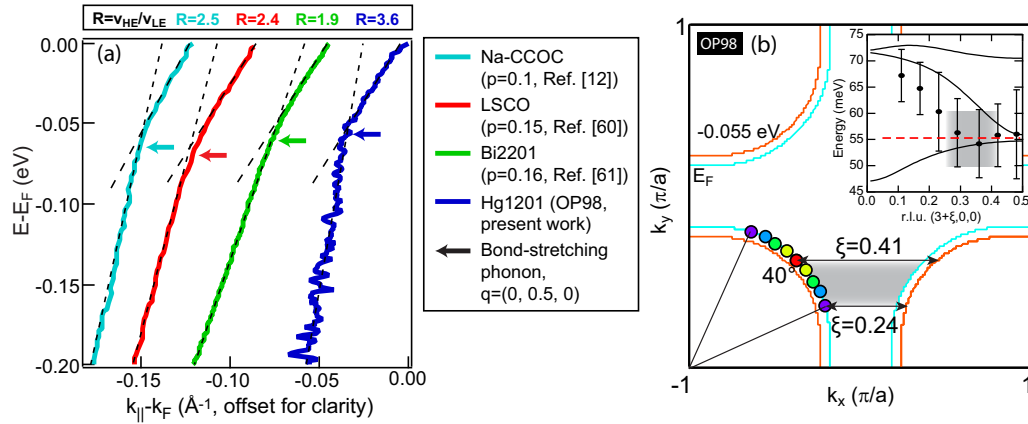
FIG. 5. Intermediate-energy kink and bond-stretching phonon. (a) Comparison of the intermediate-energy nodal kink for four single-layer cuprates near optimal doping [12,60,61] with corresponding values of the bond-stretching phonon at $\mathbf{q}=(0.5,0,0)$ [48,62–64]. Dashed lines: fits to $v_{LE}$ (low-energy velocity [20,45], meV) and $v_{HE}$ (high-energy velocity [80 200], meV). The renormalization across the intermediate-energy kink, $R \equiv v_{HE}/v_{LE}$, is indicated. Hg1201 ARPES data taken at 30 K. (b) Momentum-dependent electron-phonon coupling, schematic. Cyan: tight-binding Fermi surface for $p = 0.16$ (Ref. [39]). Orange: constant energy contour at kink energy ($-0.055$ eV). Dots on Fermi surface denote $k_F$ for cuts in Fig. 3(i). Arrows connect one constant energy contour ($E_F$) to another ($-0.055$ eV) along $(q,0,0)$ starting from node and also starting at Fermi surface angle $\theta = 20°$. Inset: dispersion of bond-stretching phonon measured by inelastic x-ray scattering from Ref. [48]. Shaded region between arrows and in inset corresponds to the same range of $\mathbf{q}$. Dotted line: observed kink energy at OP.

can be reproduced by electrons coupling primarily to the *soft* portion of the half-breathing mode—momentum transfer near $\mathbf{q} = (0.5,0,0)$ where the phonon energy is decreased from the parent-compound value. Notably, this and nearby values of $\mathbf{q}$ can connect states at the kink energy near one node to states at $E_F$ near an opposite node but is too large to connect near-antinodal states. This is shown schematically in Fig. 5(b), using the Fermi surface and observed kink energy of optimally-doped Hg1201, where both ARPES data and the measured phonon dispersion of the bond-stretching phonon is available. This momentum-dependent coupling can also produce a kink whose energy is minimally gap-shifted by the superconducting gap, as the superconducting gap near the nodes is zero or small relative to the bond-stretching mode energy.

The identity of the phonon contributing to the intermediate-energy kink is somewhat separate from this mode's role in superconductivity. The bond-stretching mode has been associated with both enhancement [74] and suppression [52,75] of $d$-wave pairing. The persistence of the kink into the over-doped, nonsuperconducting regime has also been interpreted in terms of the bond-stretching mode having no relation to superconductivity [45]. On the other hand, Hg1201 shows a stronger velocity renormalization across the intermediate-energy kink [Fig. 5(a)], an estimate of the coupling strength, than other single-layer cuprates with lower $T_c$. This velocity renormalization, $R = v_{HE}/v_{LE}$, varies among single-layer cuprates from 1.9 (Bi2201) to 3.6 (Hg1201); here, the low-energy velocity $v_{LE}$ is taken as the slope of the MDC dispersion in the [20,45] meV range, and the high-energy velocity $v_{HE}$ is the slope in the [80 200] meV range. This suggests that for Hg1201, the single-layer cuprate with the largest $T_{c,max}$, deleterious effects of the bond-stretching mode on superconductivity are minimal or fully compensated by other factors that raise $T_c$.

Finally, we turn to the *nodal* PDH structure. We first discuss general interpretations of PDH lineshapes in the cuprates and then turn specifically to this feature at the *node* in single-layer cuprates. At the antinode, the PDH lineshape is weak or absent in single-layer cuprates but ubiquitous in multi-$CuO_2$-plane compounds [16,79,80] with several component-resolved interpretations. The antinodal dip feature [54,81,82] or the entirety of the lineshape [83] has been attributed to a magnetic resonance mode. Alternately, the dip feature has also been associated with electron-phonon coupling to the $B_{1g}$ oxygen bond-buckling phonon [84,85]. The peak feature at the antinode has been associated with the superconducting condensate, as it disappears above $T_c$ [80,86] and follows the doping dependence of the superfluid density [87]. The antinodal hump feature below $T_c$ in multi-$CuO_2$-plane cuprates has been associated with the pseudogap, as it evolves into the broadly peaked lineshape defining the pseudogap above $T_c$ [86], or as a feature also related to electron-phonon coupling [3].

Near the node, a PDH similar to the present observation has been reported in Na-CCOC [12,77], and the hump feature was discussed in the context of polaron physics [88]. In that material, the nodal PDH was only reported up to 12% hole doping. A nodal PDH lineshape is also seen in nonsuperconducting Bi2201, up to $p \approx 0.105$ [46]. At optimal doping, the nodal PDH structure is not reported in Bi2201 and LSCO, with EDCs below the kink energy smoothly evolving into sharper quasiparticles above the kink energy [14,79]. In LSCO a similar feature, albeit located at systematically higher energy, has been associated with the lower Hubbard band [78].

Our results are inconsistent with an interpretation of the near-nodal dip as a sharp mode, because its energy disperses with momentum along a cut [Figs. 2(c), 2(f) and 2(i)]. Instead, the hump and the peak appear to be the fundamental spectral elements, with the dip energy reflecting their meeting point.
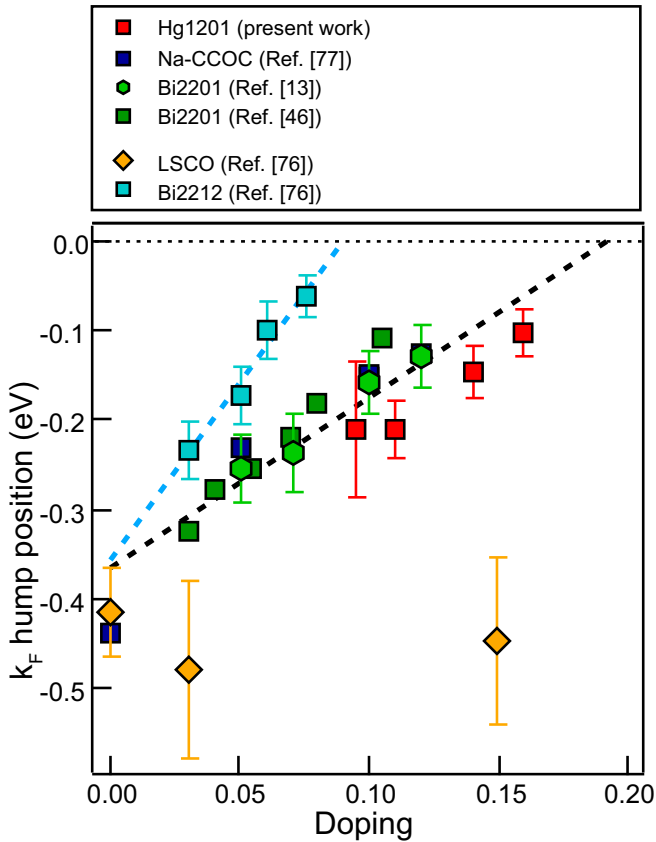
FIG. 6. Comparison of 'hump' energy scales at nodal $k_F$ for five cuprates. Additional datum for Hg1201 at $p = 0.14$ from Ref. [31]. Blue dashed line: linear fit to Bi2212 data [76]. Black dashed line: linear fit for Bi2201 [13,46], Na-CCOC [77], and Hg1201. LSCO data from Ref. [76], adapted from Ref. [78].

Additionally, the dip persists to above $T_c$ (Fig. 4(b), Ref. [12]), unlike for multi-CuO$_2$-plane cuprates, where the antinodal dip characteristically vanishes across $T_c$. We also note that in Ref. [31], a 'kink' was reported in the MDC dispersion at around 200 meV, which is likely another manifestation of the nodal hump structure in Hg1201. Robust features of strong electronic interactions typically manifest in both the MDC and EDC channels but are sometimes better visualized in one or the other, and the present feature is better quantified in EDCs.

In Fig. 6 we highlight the universality of the nodal PDH structure and its relevance to the phase diagram. We compare our result for Hg1201 with data from LSCO [78], Na-CCOC [77], Bi2201 [13,46], and Bi2212 [76]. We note that while similar spectral features are identified for all the materials, they are not necessarily interpreted the same way in the existing literature. Three systematic trends are observed: LSCO shows minimal doping dependence of the nodal hump feature. Double-layer Bi2212 exhibits the nodal PDH feature only at low doping, with an energy scale that extrapolates to zero at $p \approx 0.09$. Within error, the remaining materials, all single-layer cuprates, exhibit the same hump energy scale, which extrapolates to zero at $p \approx 0.2$.

Although Bi2212 and LSCO show a nodal PDH lineshape in certain regimes, they are outliers in overall phenomenology. Bi2212 shows this structure only in the deeply underdoped

regime, and interestingly, the hump energy extrapolates to zero near a phase boundary ($p \approx 0.09$) where a nonsuperconducting gap opens at the nodal momentum, possibly associated with spin-density wave order [89,90]. In LSCO, the nodal hump feature is thought to be doping independent because of chemical potential pinning in that compound in the underdoped regime [91].

Other single-layer cuprates where spectroscopic data are available in the underdoped regime (Bi2201, Na-CCOC, Hg1201) exhibit consistent nodal hump energy scales. This common energy scale extrapolates to zero energy around $p = 0.2$, a hole concentration identified with both a phase boundary [89,92] and percolative delocalization of the Mott-localized holes [93,94]. This suggests that the nodal hump may also be connected with the pseudogap or charge order—phenomena associated with that characteristic doping. Notably, structural/electronic inhomogeneity [95] has been identified as key to explaining many aspects of cuprate phenomenology, including doping and temperature dependence of resistivity [93,94], emergence of superconductivity on cooling [96], and the doping and temperature evolution of ARPES lineshapes [97]. The broadly-peaked nodal hump feature may be the manifestation of similar strong spatial inhomogeneity, possibly dynamic in nature [98], which the present experiment's macroscopic spot size averages out. Local-probe measurements can clarify this issue in Hg1201, as they have in Bi-based cuprates. We also note that optical probes have reported a broad continuum of excitations at energies of several hundred meV, with purported relevance for the pairing mechanism, and the phenomenology of these features is consistent with the nodal PDH [22,99]. At optimal doping, the momentum dependence of the hump energy scale nearly follows a $d$-wave form and extrapolates to an antinodal energy scale of $\approx 300$ meV [Fig. 4(d)], which is consistent with the maximum of the broad continuum of excitations derived from optics measurements at the same doping [22]. Taken together, the present results and the discussed literature suggest a cooperative interplay between dynamic lattice and electronic effects as well as an important role played by inherent inhomogeneity.

## V. CONCLUSIONS

Hg1201 is a model cuprate which has been at the forefront of new insights about high-temperature superconductivity via many experimental techniques but has heretofore received limited investigation via surface spectroscopies such as ARPES. In addressing this omission, we have identified three energy scales of interactions in Hg1201 with implications for understanding electron-phonon coupling in cuprates and connections to the phase diagram. The low-energy (11 meV) and intermediate-energy (55 meV) kinks reflect electron-phonon coupling, with the former most consistent with coupling to out-of-plane Ba modes and the latter reflecting coupling to the in-plane oxygen half-breathing mode. Both interactions may involve large momentum transfer. We note the possibility that the overall broad intermediate-energy feature contains additional electronic contributions. At higher binding energy, a PDH structure is observed at the node, with connections to a previously reported broad continuum of excitations and the phase boundary of the pseudogap and/or charge order.

As compared to single-layer cuprates with lower $T_c$, some differences exist with regards to low-energy many-body interactions. The coupling to the low- and intermediate-energy kinks appears to be stronger at the same doping in Hg1201. This points to electron-phonon coupling as a possible means of enhancing $T_c$ in single-layer cuprates. Additionally, while the nodal PDH structure is present in the underdoped regime in most single-layer cuprates, this spectral feature persists to optimal doping in Hg1201, which may suggest an intervening competing phase in lower-$T_c$ members.

This work also establishes points of universality among cuprates. With this observation of the low-energy kink outside of the Bi family of cuprates, strong coupling to subgap phonons appears to be a universal aspect of cuprate phenomenology, although the identity of the phonon and the nature of the coupling (large vs small **q**) may differ among different materials. The intermediate-energy kink has long been known to be ubiquitous in cuprates. The present results highlight that the bond-stretching phonon at **q** $\approx (0.5, 0, 0)$ can reproduce the phenomenology of the intermediate-energy kink in all single layer cuprates where both ARPES and phonon dispersion data are available. Finally, a nodal PDH structure appears to be ubiquitous in single-layer cuprates with a common doping dependence among several compounds but with properties distinct from the antinodal PDH structure previously established in multiple-CuO$_2$-plane cuprates. Nevertheless, the nodal PDH may also be connected to the pseudogap, highlighting that this enigmatic phase may be relevant to nodal and near-nodal physics.

## APPENDIX: SURFACE TERMINATION

While ARPES is a technique that allows direct visualization of the band structure, the observed spectrum shows strong dependence on sample surface structure [100,101]. Typically, one obtains a chemically pure surface by
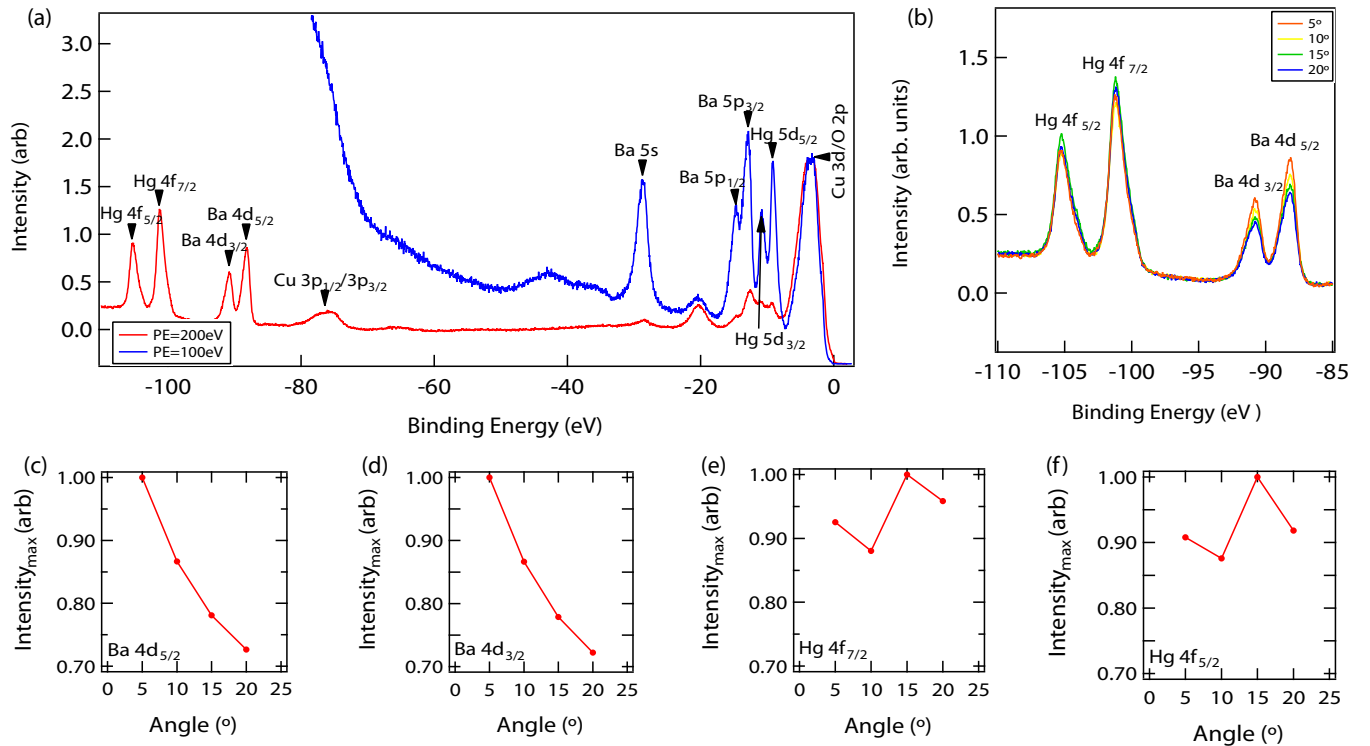


FIG. 7. (a) Core levels of Hg1201 at photon energies (PE) of 100 eV and 200 eV taken at normal incidence. (b) Hg $4f$ and Ba $4d$ core levels at different polar angles taken with 200 eV. (c)–(f) Polar angle dependence of the peak intensities for various core levels normalized to the maximum in each series.

mechanical cleaving—gluing a top post on the sample and knocking it off in ultrahigh vacuum before measurement. Hg1201, due to the absence of a neutral cleavage plane [17], has no obvious preferred termination upon cleaving. In the absence of atomic-scale studies of Hg1201 in the literature, surface terminations can be inferred from photoemission studies.

Angle-resolved x-ray photoemission spectroscopy (AR-XPS) is a technique that probes core levels of elements in a sample up to different depths by varying the angle between detector and the surface. Depth sensitivity in photoemission is limited by the mean free path of the electrons after they encounter an optical excitation in the solid [102], but before they reach and leave the surface [103]. By varying the angle of the surface normal of the sample with respect to the direction of the detector (the photoemission angle), electrons from deeper inside the sample must travel longer distances through the sample before reaching the sample surface, causing them to be scattered more than electrons located closer to the surface. To a first approximation, the photoemission intensity for a homogeneous sample as a function of depth and photoemission angle can be modelled as

$$I = I_{z=0} \exp\left( \frac{-z}{\lambda \cos\theta} \right), \qquad (A1)$$

where $z$ is the depth of origin for the electron from the surface, $\lambda$ is the inelastic mean free path, and $\theta$ is the photoemission angle. While the model does not account for multiple scattering, elastic scattering or nonisotropic effects, the principle that the electrons that reach the detector predominantly originate from a depth of the order of $\lambda$ still holds [104]. Based on Eq. (A1), atoms located on the surface are less affected by

the orientation of the surface, while atoms located deeper into the sample originate fewer photoelectrons at oblique photoemission angles due to higher scattering.

Figure 7(a) shows the relevant core levels on Hg1201 obtained at photon energies of 100 eV and 200 eV. Both spectra have been rescaled with respect to the Cu-O valence band peak for comparison. We observe a strong photon energy dependence on the relative intensities of the core levels between the two spectra. The following discussion focuses only on the deeper Hg and Ba core levels($4f$ and $4d$), measured with 200 eV photon energy, for an angle-dependent study. Figure 7(b) details the XPS intensities of the Ba $4d$ and Hg $4f$ at different photoemission angles between the surface normal and the detector. We observe a systematic decrease in the peak intensities of the Ba core levels with increasing photoemission angle. The maximum intensities are then obtained by fitting Lorentzians to each of the peaks. The intensities are then normalized to the maximum within the angle series and plotted in Figs. 7(c)–7(f). The data show a steady decrease in intensities of the peaks for the Ba core levels while showing no monotonic trend for the Hg core levels. This suggests that Ba atoms are located further from the surface than Hg atoms.

These data are consistent with cleavage close to the Hg plane, and further from the Ba plane, specifically at the Hg-O bonds. Due to the symmetry of the O-Hg-O barbells, both bonds above and below a Hg atom are equally likely to be broken resulting in a mixed O and Hg surface termination. This effectively gives a charge-neutral cleaved surface, possibly explaining why as-cleaved Hg1201 does not exhibit polar catastrophe as as-cleaved YBCO [31,105]. Confirmation of the same will require further atomic resolved experiments not yet available in literature, but this work provides a photoemission-based guide.

[1] C. Howald, P. Fournier, and A. Kapitulnik, Phys. Rev. B **64**, 100504(R) (2001).

[2] K. M. Lang, V. Madhavan, J. E. Hoffman, E. W. Hudson, H. Eisaki, S. Uchida, and J. C. Davis, Nature (London) **415**, 412 (2002).

[3] T. Cuk, D. H. Lu, X. J. Zhou, Z.-X. Shen, T. P. Devereaux, and N. Nagaosa, Phys. Status Solidi (b) **242**, 11 (2005).

[4] M. Hashimoto, I. M. Vishik, R.-H. He, T. P. Devereaux, and Z.-X. Shen, Nat. Phys. **10**, 483 (2014).

[5] H. Anzai, M. Arita, H. Namatame, M. Taniguchi, M. Ishikado, K. Fujita, S. Ishida, S. Uchida, and A. Ino, Sci. Rep. **7**, 4830 (2017).

[6] H. Eisaki, N. Kaneko, D. L. Feng, A. Damascelli, P. K. Mang, K. M. Shen, Z.-X. Shen, and M. Greven, Phys. Rev. B **69**, 064512 (2004).

[7] H. Sakakibara, H. Usui, K. Kuroki, R. Arita, and H. Aoki, Phys. Rev. B **85**, 064501 (2012).

[8] E. Pavarini, I. Dasgupta, T. Saha-Dasgupta, O. Jepsen, and O. K. Andersen, Phys. Rev. Lett. **87**, 047003 (2001).

[9] S. Teranishi, K. Nishiguchi, and K. Kusakabe, J. Phys. Soc. Jpn. **87**, 114701 (2018).

[10] C. E. Matt, D. Sutter, A. M. Cook, Y. Sassa, M. Månsson, O. Tjernberg, L. Das, M. Horio, D. Destraz, C. G. Fatuzzo,

K. Hauser, M. Shi, M. Kobayashi, V. N. Strocov, T. Schmitt, P. Dudin, M. Hoesch, S. Pyon, T. Takayama, H. Takagi, O. J. Lipscombe, S. M. Hayden, T. Kurosawa, N. Momono, M. Oda, T. Neupert, and J. Chang, Nat. Commun. **9**, 972 (2018).

[11] K. P. Kramer, M. Horio, S. S. Tsirkin, Y. Sassa, K. Hauser, C. E. Matt, D. Sutter, A. Chikina, N. B. M. Schröter, J. A. Krieger, T. Schmitt, V. N. Strocov, N. C. Plumb, M. Shi, S. Pyon, T. Takayama, H. Takagi, T. Adachi, T. Ohgi, T. Kawamata, Y. Koike, T. Kondo, O. J. Lipscombe, S. M. Hayden, M. Ishikado, H. Eisaki, T. Neupert, and J. Chang, Phys. Rev. B **99**, 224509 (2019).

[12] F. Ronning, T. Sasagawa, Y. Kohsaka, K. M. Shen, A. Damascelli, C. Kim, T. Yoshida, N. P. Armitage, D. H. Lu, D. L. Feng, L. L. Miller, H. Takagi, and Z.-X. Shen, Phys. Rev. B **67**, 165101 (2003).

[13] M. Hashimoto, T. Yoshida, H. Yagi, M. Takizawa, A. Fujimori, M. Kubota, K. Ono, K. Tanaka, D. H. Lu, Z.-X. Shen, S. Ono, and Y. Ando, Phys. Rev. B **77**, 094516 (2008).

[14] T. Yoshida, X. J. Zhou, D. H. Lu, S. Komiya, Y. Ando, H. Eisaki, T. Kakeshita, S. Uchida, Z. Hussain, Z.-X. Shen, and A. Fujimori, J. Phys.: Condens. Matter **19**, 125209 (2007).

[15] M. Platé, J. D. F. Mottershead, I. S. Elfimov, D. C. Peets, R. Liang, D. A. Bonn, W. N. Hardy, S. Chiuzbaian, M. Falub,

M. Shi, L. Patthey, and A. Damascelli, Phys. Rev. Lett. **95**, 077001 (2005).

[16] W. S. Lee, K. Tanaka, I. M. Vishik, D. H. Lu, R. G. Moore, H. Eisaki, A. Iyo, T. P. Devereaux, and Z. X. Shen, Phys. Rev. Lett. **103**, 067003 (2009).

[17] N. Barišić, Y. Li, X. Zhao, Y.-C. Cho, G. Chabot-Couture, G. Yu, and M. Greven, Phys. Rev. B **78**, 054518 (2008).

[18] A. Schilling, M. Cantoni, J. D. Guo, and H. R. Ott, Nature (London) **363**, 56 (1993).

[19] N. Barišić, M. K. Chan, Y. Li, G. Yu, X. Zhao, M. Dressel, A. Smontara, and M. Greven, Proc. Natl. Acad. Sci. USA **110**, 12235 (2013).

[20] N. Doiron-Leyraud, S. Lepault, O. Cyr-Choinière, B. Vignolle, G. Grissonnanche, F. Laliberté, J. Chang, N. Barišić, M. K. Chan, L. Ji, X. Zhao, Y. Li, M. Greven, C. Proust, and L. Taillefer, Phys. Rev. X **3**, 021019 (2013).

[21] H. Murayama, Y. Sato, R. Kurihara, S. Kasahara, Y. Mizukami, Y. Kasahara, H. Uchiyama, A. Yamamoto, E. G. Moon, J. Cai, J. Freyermuth, M. Greven, T. Shibauchi, and Y. Matsuda, Nat. Commun. **10**, 3282 (2019).

[22] E. van Heumen, E. Muhlethaler, A. B. Kuzmenko, H. Eisaki, W. Meevasana, M. Greven, and D. van der Marel, Phys. Rev. B **79**, 184512 (2009).

[23] M. S. Grbić, N. Barišić, A. Dulčić, I. Kupčić, Y. Li, X. Zhao, G. Yu, M. Dressel, M. Greven, and M. Požek, Phys. Rev. B **80**, 094511 (2009).

[24] Y. Li, V. Balédent, N. Barišić, Y. Cho, B. Fauqué, Y. Sidis, G. Yu, X. Zhao, P. Bourges, and M. Greven, Nature (London) **455**, 372 (2008).

[25] M. K. Chan, Y. Tang, C. J. Dorow, J. Jeong, L. Mangin-Thro, M. J. Veit, Y. Ge, D. L. Abernathy, Y. Sidis, P. Bourges, and M. Greven, Phys. Rev. Lett. **117**, 277002 (2016).

[26] M. K. Chan, C. J. Dorow, L. Mangin-Thro, Y. Tang, Y. Ge, M. J. Veit, G. Yu, X. Zhao, A. D. Christianson, J. T. Park, Y. Sidis, P. Steffens, D. L. Abernathy, P. Bourges, and M. Greven, Nat. Commun. **7**, 10819 (2016).

[27] L. Lu, X. Zhao, J. N. Hancock, G. Chabot-Couture, N. Kaneko, O. P. Vajk, G. Yu, S. Grenier, Y. J. Kim, D. Casa, T. Gog, and M. Greven, Phys. Rev. Lett. **95**, 217003 (2005).

[28] W. Tabis, Y. Li, M. L. Tacon, L. Braicovich, A. Kreyssig, M. Minola, G. Dellea, E. Weschke, M. J. Veit, M. Ramazanoglu, A. I. Goldman, T. Schmitt, G. Ghiringhelli, N. Barišić, M. K. Chan, C. J. Dorow, G. Yu, X. Zhao, B. Keimer, and M. Greven, Nat. Commun. **5**, 5875 (2014).

[29] W. Tabis, B. Yu, I. Bialo, M. Bluschke, T. Kolodziej, A. Kozlowski, E. Blackburn, K. Sen, E. M. Forgan, M. v. Zimmermann, Y. Tang, E. Weschke, B. Vignolle, M. Hepting, H. Gretarsson, R. Sutarto, F. He, M. Le Tacon, N. Barišić, G. Yu, and M. Greven, Phys. Rev. B **96**, 134510 (2017).

[30] Y. Li, M. Le Tacon, Y. Matiks, A. V. Boris, T. Loew, C. T. Lin, L. Chen, M. K. Chan, C. Dorow, L. Ji, N. Barišić, X. Zhao, M. Greven, and B. Keimer, Phys. Rev. Lett. **111**, 187001 (2013).

[31] I. M. Vishik, N. Barišić, M. K. Chan, Y. Li, D. D. Xia, G. Yu, X. Zhao, W. S. Lee, W. Meevasana, T. P. Devereaux, M. Greven, and Z.-X. Shen, Phys. Rev. B **89**, 195141 (2014).

[32] J. D. Rameau, H.-B. Yang, G. D. Gu, and P. D. Johnson, Phys. Rev. B **80**, 184513 (2009).

[33] I. M. Vishik, W. S. Lee, F. Schmitt, B. Moritz, T. Sasagawa, S. Uchida, K. Fujita, S. Ishida, C. Zhang, T. P. Devereaux, and Z. X. Shen, Phys. Rev. Lett. **104**, 207002 (2010).

[34] T. Kondo, Y. Nakashima, W. Malaeb, Y. Ishida, Y. Hamaya, T. Takeuchi, and S. Shin, Phys. Rev. Lett. **110**, 217006 (2013).

[35] N. C. Plumb, T. J. Reber, J. D. Koralek, Z. Sun, J. F. Douglas, Y. Aiura, K. Oka, H. Eisaki, and D. S. Dessau, Phys. Rev. Lett. **105**, 046402 (2010).

[36] S. Johnston, I. M. Vishik, W. S. Lee, F. Schmitt, S. Uchida, K. Fujita, S. Ishida, N. Nagaosa, Z. X. Shen, and T. P. Devereaux, Phys. Rev. Lett. **108**, 166404 (2012).

[37] X. Zhao, G. Yu, Y.-C. Cho, G. Chabot-Couture, N. Barišić, P. Bourges, N. Kaneko, Y. Li, L. Lu, E. Motoyama, O. Vajk, and M. Greven, Adv. Mater. **18**, 3243 (2006).

[38] A. Yamamoto, W.-Z. Hu, and S. Tajima, Phys. Rev. B **63**, 024504 (2000).

[39] T. Das, Phys. Rev. B **86**, 054518 (2012).

[40] $E_k = -2t[\cos(k_x a) + \cos(k_y a)] - 4t'[\cos(k_x a)\cos(k_y a)] - 2t''$ $[\cos(2k_x a) + \cos(2k_y a)] - 4t'''[\cos(2k_x a)\cos(k_y a) + \cos(k_x a)$ $\cos(2k_y a)] - \mu$ where $(t, t', t'', t''') = (0.46, -0.105, 0.08, -0.02)$ and $\mu$ is adjusted to nominal doping.

[41] See Supplemental Material at http://link.aps.org/supplemental/10.1103/PhysRevB.102.205109 for tight-binding calculations and additional photoemission data.

[42] P. D. Johnson and T. Valla, in *Very High Resolution Photoelectron Spectroscopy* (Springer, Berlin/Heidelberg, 2007), pp. 55–84.

[43] J. He, W. Zhang, J. M. Bok, D. Mou, L. Zhao, Y. Peng, S. He, G. Liu, X. Dong, J. Zhang, J. S. Wen, Z. J. Xu, G. D. Gu, X. Wang, Q. Peng, Z. Wang, S. Zhang, F. Yang, C. Chen, Z. Xu, H.-Y. Choi, C. M. Varma, and X. J. Zhou, Phys. Rev. Lett. **111**, 107005 (2013).

[44] W. S. Lee, W. Meevasana, S. Johnston, D. H. Lu, I. M. Vishik, R. G. Moore, H. Eisaki, N. Kaneko, T. P. Devereaux, and Z. X. Shen, Phys. Rev. B **77**, 140504(R) (2008).

[45] S. R. Park, Y. Cao, Q. Wang, M. Fujita, K. Yamada, S.-K. Mo, D. S. Dessau, and D. Reznik, Phys. Rev. B **88**, 220503(R) (2013).

[46] Y. Peng, J. Meng, D. Mou, J. He, L. Zhao, Y. Wu, G. Liu, X. Dong, S. He, J. Zhang, X. Wang, Q. Peng, Z. Wang, S. Zhang, F. Yang, C. Chen, Z. Xu, T. K. Lee, and X. J. Zhou, Nat. Commun. **4**, 2459 (2013).

[47] M. d'Astuto, A. Mirone, P. Giura, D. Colson, A. Forget, and M. Krisch, J. Phys.: Condens. Matter **15**, 8827 (2003).

[48] H. Uchiyama, A. Q. R. Baron, S. Tsutsui, Y. Tanaka, W.-Z. Hu, A. Yamamoto, S. Tajima, and Y. Endoh, Phys. Rev. Lett. **92**, 197005 (2004).

[49] X. Zhou, M. Cardona, C. Chu, Q. Lin, S. Loureiro, and M. Marezio, Physica C **270**, 193 (1996).

[50] A. Lanzara, P. V. Bogdanov, X. J. Zhou, S. A. Kellar, D. L. Feng, E. D. Lu, T. Yoshida, H. Eisaki, A. Fujimori, K. Kishio, J. I. Shimoyama, T. Noda, S. Uchida, Z. Hussain, and Z. X. Shen, Nature (London) **412**, 510 (2001).

[51] S. Johnston, W. S. Lee, Y. Chen, E. A. Nowadnick, B. Moritz, Z.-X. Shen, and T. P. Devereaux, Adv. Condens. Matter Phys. **2010**, 968304 (2010).

[52] S. Johnston, F. Vernay, B. Moritz, Z.-X. Shen, N. Nagaosa, J. Zaanen, and T. P. Devereaux, Phys. Rev. B **82**, 064513 (2010).

[53] A. A. Kordyuk, S. V. Borisenko, V. B. Zabolotnyy, J. Geck, M. Knupfer, J. Fink, B. Büchner, C. T. Lin, B. Keimer, H. Berger, A. V. Pan, S. Komiya, and Y. Ando, Phys. Rev. Lett. **97**, 017002 (2006).

[54] T. Dahm, V. Hinkov, S. V. Borisenko, A. A. Kordyuk, V. B. Zabolotnyy, J. Fink, B. Büchner, D. J. Scalapino, W. Hanke, and B. Keimer, Nat. Phys. **5**, 217 (2009).

[55] J. Bauer and G. Sangiovanni, Phys. Rev. B **82**, 184535 (2010).

[56] A. V. Chubukov and M. R. Norman, Phys. Rev. B **70**, 174505 (2004).

[57] K. Matsuyama, E. Perepelitsky, and B. S. Shastry, Phys. Rev. B **95**, 165435 (2017).

[58] Y. Li, G. Yu, M. K. Chan, V. Balédent, Y. Li, N. Barišić, X. Zhao, K. Hradil, R. A. Mole, Y. Sidis, P. Steffens, P. Bourges, and M. Greven, Nat. Phys. **8**, 404 (2012).

[59] B. Yu, W. Tabis, I. Bialo, F. Yakhou, N. B. Brookes, Z. Anderson, Y. Tang, G. Yu, and M. Greven, Phys. Rev. X **10**, 021059 (2020).

[60] X. J. Zhou, T. Yoshida, A. Lanzara, P. V. Bogdanov, S. A. Kellar, K. M. Shen, W. L. Yang, F. Ronning, T. Sasagawa, T. Kakeshita, H. Noda, H. Eisaki, S. Uchida, C. T. Lin, F. Zhou, J. W. Xiong, W. X. Ti, Z. X. Zhao, A. Fujimori, Z. Hussain, and Z. X. Shen, Nature (London) **423**, 398 (2003).

[61] K. Sato, H. Iwasawa, N. C. Plumb, T. Masui, Y. Yoshida, H. Eisaki, H. Bando, A. Ino, M. Arita, K. Shimada, H. Namatame, M. Taniguchi, S. Tajima, Y. Nishihara, D. S. Dessau, and Y. Aiura, Phys. Rev. B **80**, 212501 (2009).

[62] M. d'Astuto, I. Yamada, P. Giura, L. Paulatto, A. Gauzzi, M. Hoesch, M. Krisch, M. Azuma, and M. Takano, Phys. Rev. B **88**, 014522 (2013).

[63] L. Pintschovius, D. Reznik, and K. Yamada, Phys. Rev. B **74**, 174514 (2006).

[64] J. Graf, M. d'Astuto, C. Jozwiak, D. R. Garcia, N. L. Saini, M. Krisch, K. Ikeuchi, A. Q. R. Baron, H. Eisaki, and A. Lanzara, Phys. Rev. Lett. **100**, 227002 (2008).

[65] G. Yu, Y. Li, E. M. Motoyama, and M. Greven, Nat. Phys. **5**, 873 (2009).

[66] Y. Li, V. Balédent, G. Yu, N. Barišić, K. Hradil, R. A. Mole, Y. Sidis, P. Steffens, X. Zhao, P. Bourges, and M. Greven, Nature (London) **468**, 283 (2010).

[67] L. Pintschovius and M. Braden, Phys. Rev. B **60**, R15039 (1999).

[68] I. Ahmadova, T. C. Sterling, A. C. Sokolik, D. L. Abernathy, M. Greven, and D. Reznik, Phys. Rev. B **101**, 184508 (2020).

[69] A. W. Sandvik, D. J. Scalapino, and N. E. Bickers, Phys. Rev. B **69**, 094523 (2004).

[70] I. Vishik, Low energy excitations in cuprate high temperature superconductors: Angle-resolved photoemission spectroscopy studies, Ph.D. thesis, Stanford University, 2013.

[71] A. Lanzara, P. Bogdanov, X. Zhou, N. Kaneko, H. Eisaki, M. Greven, Z. Hussain, and Z. Shen, J. Phys. Chem. Solids **67**, 239 (2006).

[72] L. Zhao, J. Wang, J. Shi, W. Zhang, H. Liu, J. Meng, G. Liu, X. Dong, J. Zhang, W. Lu, G. Wang, Y. Zhu, X. Wang, Q. Peng, Z. Wang, S. Zhang, F. Yang, C. Chen, Z. Xu, and X. J. Zhou, Phys. Rev. B **83**, 184515 (2011).

[73] T. P. Devereaux, T. Cuk, Z.-X. Shen, and N. Nagaosa, Phys. Rev. Lett. **93**, 117004 (2004).

[74] S. Ishihara and N. Nagaosa, Phys. Rev. B **69**, 144520 (2004).

[75] T. Sakai, D. Poilblanc, and D. J. Scalapino, Phys. Rev. B **55**, 8445 (1997).

[76] K. Tanaka, T. Yoshida, K. M. Shen, D. H. Lu, W. S. Lee, H. Yagi, A. Fujimori, Z.-X. Shen, Risdiana, T. Fujii, and I. Terasaki, Phys. Rev. B **81**, 125115 (2010).

[77] K. M. Shen, F. Ronning, D. H. Lu, W. S. Lee, N. J. C. Ingle, W. Meevasana, F. Baumberger, A. Damascelli, N. P. Armitage, L. L. Miller, Y. Kohsaka, M. Azuma, M. Takano, H. Takagi, and Z.-X. Shen, Phys. Rev. Lett. **93**, 267002 (2004).

[78] A. Ino, C. Kim, M. Nakamura, T. Yoshida, T. Mizokawa, A. Fujimori, Z.-X. Shen, T. Kakeshita, H. Eisaki, and S. Uchida, Phys. Rev. B **65**, 094504 (2002).

[79] J. Wei, Y. Zhang, H. W. Ou, B. P. Xie, D. W. Shen, J. F. Zhao, L. X. Yang, M. Arita, K. Shimada, H. Namatame, M. Taniguchi, Y. Yoshida, H. Eisaki, and D. L. Feng, Phys. Rev. Lett. **101**, 097005 (2008).

[80] D. L. Feng, A. Damascelli, K. M. Shen, N. Motoyama, D. H. Lu, H. Eisaki, K. Shimizu, J.-i. Shimoyama, K. Kishio, N. Kaneko, M. Greven, G. D. Gu, X. J. Zhou, C. Kim, F. Ronning, N. P. Armitage, and Z.-X. Shen, Phys. Rev. Lett. **88**, 107001 (2002).

[81] J. C. Campuzano, H. Ding, M. R. Norman, H. M. Fretwell, M. Randeria, A. Kaminski, J. Mesot, T. Takeuchi, T. Sato, T. Yokoya, T. Takahashi, T. Mochiku, K. Kadowaki, P. Guptasarma, D. G. Hinks, Z. Konstantinovic, Z. Z. Li, and H. Raffy, Phys. Rev. Lett. **83**, 3709 (1999).

[82] A. D. Gromko, A. V. Fedorov, Y.-D. Chuang, J. D. Koralek, Y. Aiura, Y. Yamaguchi, K. Oka, Y. Ando, and D. S. Dessau, Phys. Rev. B **68**, 174520 (2003).

[83] A. Abanov and A. V. Chubukov, Phys. Rev. Lett. **83**, 1652 (1999).

[84] T. Cuk, F. Baumberger, D. H. Lu, N. Ingle, X. J. Zhou, H. Eisaki, N. Kaneko, Z. Hussain, T. P. Devereaux, N. Nagaosa, and Z.-X. Shen, Phys. Rev. Lett. **93**, 117003 (2004).

[85] Y. He, M. Hashimoto, D. Song, S.-D. Chen, J. He, I. M. Vishik, B. Moritz, D.-H. Lee, N. Nagaosa, J. Zaanen, T. P. Devereaux, Y. Yoshida, H. Eisaki, D. H. Lu, and Z.-X. Shen, Science **362**, 62 (2018).

[86] M. Hashimoto, E. A. Nowadnick, R.-H. He, I. M. Vishik, B. Moritz, Y. He, K. Tanaka, R. G. Moore, D. Lu, Y. Yoshida, M. Ishikado, T. Sasagawa, K. Fujita, S. Ishida, S. Uchida, H. Eisaki, Z. Hussain, T. P. Devereaux, and Z.-X. Shen, Nat. Mater. **14**, 37 (2014).

[87] D. L. Feng, D. H. Lu, K. M. Shen, C. Kim, H. Eisaki, A. Damascelli, R. Yoshizaki, J.-i. Shimoyama, K. Kishio, G. D. Gu, S. Oh, A. Andrus, J. O'Donnell, J. N. Eckstein, and Z.-X. Shen, Science **289**, 277 (2000).

[88] K. M. Shen, F. Ronning, W. Meevasana, D. H. Lu, N. J. C. Ingle, F. Baumberger, W. S. Lee, L. L. Miller, Y. Kohsaka, M. Azuma, M. Takano, H. Takagi, and Z.-X. Shen, Phys. Rev. B **75**, 075115 (2007).

[89] I. M. Vishik, M. Hashimoto, R.-H. He, W.-S. Lee, F. Schmitt, D. Lu, R. G. Moore, C. Zhang, W. Meevasana, T. Sasagawa, S. Uchida, K. Fujita, S. Ishida, M. Ishikado, Y. Yoshida, H. Eisaki, Z. Hussain, T. P. Devereaux, and Z.-X. Shen, Proc. Natl. Acad. Sci. USA **109**, 18332 (2012).

[90] G. Drachuck, E. Razzoli, G. Bazalitski, A. Kanigel, C. Niedermayer, M. Shi, and A. Keren, Nat. Commun. **5**, 3390 (2014).

[91] A. Ino, T. Mizokawa, A. Fujimori, K. Tamasaku, H. Eisaki, S. Uchida, T. Kimura, T. Sasagawa, and K. Kishio, Phys. Rev. Lett. **79**, 2101 (1997).

[92] B. Michon, C. Girod, S. Badoux, J. Kačmarčík, Q. Ma, M. Dragomir, H. A. Dabkowska, B. D. Gaulin, J. S. Zhou, S. Pyon, T. Takayama, H. Takagi, S. Verret, N. Doiron-Leyraud, C. Marcenat, L. Taillefer, and T. Klein, Nature (London) **567**, 218 (2019).

[93] D. Pelc, P. Popčević, M. Požek, M. Greven, and N. Barišić, Sci. Adv. **5**, eaau4538 (2019).

[94] D. Pelc, M. J. Veit, C. J. Dorow, Y. Ge, N. Barišić, and M. Greven, Phys. Rev. B **102**, 075114 (2020).

[95] J. Krumhansl, in *Lattice Effects in High-Tc Superconductors* (World Scientific, Santa Fe, New Mexico, 1992), pp. 503–516.

[96] D. Pelc, Z. Anderson, B. Yu, C. Leighton, and M. Greven, Nat. Commun. **10**, 2729 (2019).

[97] N. Zaki, H.-B. Yang, J. D. Rameau, P. D. Johnson, H. Claus, and D. G. Hinks, Phys. Rev. B **96**, 195163 (2017).

[98] X. Chen, J. Dong, and X. Li, npj Comput. Mater. **6**, 103 (2020).

[99] S. Dal Conte, C. Giannetti, G. Coslovich, F. Cilento, D. Bossini, T. Abebaw, F. Banfi, G. Ferrini, H. Eisaki, M. Greven, A. Damascelli, D. van der Marel, and F. Parmigiani, Science **335**, 1600 (2012).

[100] K. R. Knox, A. Locatelli, M. B. Yilmaz, D. Cvetko, T. O. Menteş, M. A. Niño, P. Kim, A. Morgante, and R. M. Osgood, Phys. Rev. B **84**, 115401 (2011).

[101] T. Fauster, C. Reuß, I. L. Shumay, M. Weinelt, F. Theilmann, and A. Goldmann, Phys. Rev. B **61**, 16168 (2000).

[102] M. P. Seah and W. A. Dench, Surf. Interface Anal. **1**, 2 (1979).

[103] S. V. Merzlikin, N. N. Tolkachev, T. Strunskus, G. Witte, T. Glogowski, C. Wöll, and W. Grünert, Surf. Sci. **602**, 755 (2008).

[104] P. J. Cumpson, in *Surface Analysis by Auger and X-ray Photoelectron Spectroscopy* (IMPublications, Chichester, UK and SurfaceSpectra, Manchester, UK, 2003), pp. 651–674.

[105] M. A. Hossain, J. D. F. Mottershead, D. Fournier, A. Bostwick, J. L. McChesney, E. Rotenberg, R. Liang, W. N. Hardy, G. A. Sawatzky, I. S. Elfimov, D. A. Bonn, and A. Damascelli, Nat. Phys. **4**, 527 (2008).